integrated values of the main peak were calculated in this case using the assumption that the angular dependence of the diffuse scattering intensity has no peculiarities and can be approximated by the linear function in the angular range of the main peak. The accuracy of the integrated values were estimated as 10-15%. The tails of the TCD curve (2) fall sharply with the increase of $|\alpha|$ and at $\alpha > 0$ one can see a weak maximum which is due to the deformation of the layer by the activated implanted B atoms. The angular position of this maximum allows one to evaluate the average lattice deformation of the layer as $\Delta d/d \simeq -2{\cdot}8 \times 10^{-4}$. It is impossible to obtain quantitative information of this kind using the DCD curve (1). As follows from kinematical theory, a sharp decrease of the TCD curve intensity is connected with the layer lattice disorder, described by the small value of the Debye-Waller factor $\exp(-W)$ (see, for example, Afanasev, Aleksandrov, Imamov, Lomov & Zavyalova, 1984).

Therefore, for sample (2) the RC measured by the DCD method is the angular dependence of the sum of the intensities of the strong diffuse waves and the extremely weak coherent wave. The TCD method allows one to measure a weak coherent component on the background of an intense diffuse scattering, which can be two or three orders of magnitude higher than the coherent one (Kazimirov, Kovalchuk & Kohn, 1987).

The authors thank S. Yu. Shiryaev for supplying the samples and for useful discussions.

References

AFANASEV, A. M., ALEKSANDROV, P. A., IMAMOV, R. M., LOMOV, A. A. & ZAVYALOVA, A. A. (1984). *Acta Cryst.* **A40**, 352-355.
AFANASEV, A. M., KAGAN, Y. M. & CHUKOVSKII, F. N. (1968). *Phys. Status Solidi*, **28**, 287-294.
AFANASEV, A. M., KOVALCHUK, M. V., KOVEV, E. K. & KOHN, V. G. (1977). *Phys. Status Solidi A*, **42**, 415-422.
BURGEAT, J. & TAUPIN, D. (1968). *Acta Cryst.* **A24**, 99-102.
CEMBALI, F., SERVIDORI, M., GABILLI, E. & LOTTI, R. (1985). *Phys. Status Solidi A*, **87**, 225.
CEMBALI, F., SERVIDORI, M., SOLMI, S., SOUREK, Z., WINTER, U. & ZAUMSEIL, P. (1986). *Phys. Status Solidi A*, **98**, 511-516.
FUKUHARA, A. & TAKANO, Y. (1977). *Acta Cryst.* **A33**, 137-142.
IIDA, A. & KOHRA, K. (1979). *Phys. Status Solidi A*, **51**, 533-542.
KAZIMIROV, A. YU., KOVALCHUK, M. V. & KOHN, F. G. (1987). *Metallofizica*, **9**, 54-58.
KOHN, V. G. (1970). *Sov. Phys. Crystallogr.* **15**, 14-17.
KOHN, V. G., KOVALCHUK, M. V., IMAMOV, R. M. & LOBANOVICH, E. F. (1981). *Phys. Status Solidi A*, **64**, 435-442.
KOHN, V. G., PRILEPSKY, M. V. & SUKHODREVA, I. M. (1984). *Poverkhn.* pp. 122-128.
KYUTT, R. N., PETRASHEN, P. V. & SOROKIN, L. M. (1980). *Phys. Status Solidi A*, **60**, 381-389.
PINSKER, Z. G. (1978). *Dynamical Scattering of X-rays in Crystals.* Heidelberg, New York: Springer-Verlag.
SPERIOSU, V. S., GLASS, H. L. & KOBAYASHI, T. (1979). *Appl. Phys. Lett.* **34**, 539-542.
ZAUMSEIL, P. (1985). *Phys. Status Solidi A*, **91**, 31.
ZAUMSEIL, P., WINTER, U., CEMBALI, F., SERVIDORI, M. & SOUREK, Z. (1987). *Phys. Status Solidi A*, **100**, 95-104.

Acta Cryst. (1990). **A46**, 649-656

X-ray Standing Waves in the Laue Case – Location of Impurity Atoms

BY A. YU. KAZIMIROV AND M. V. KOVALCHUK

A. V. Shubnikov Institute of Crystallography of the Academy of Sciences of the USSR, Leninsky Prospect 59, *Moscow* 117333, *USSR*

AND V. G. KOHN

I. V. Kurchatov Institute of Atomic Energy, Kurchatov Square 46, *Moscow* 123182, *USSR*

(*Received* 17 *February* 1989; *accepted* 12 *February* 1990)

Abstract

Impurity-atom fluorescence excited by X-ray standing waves in the Laue case of X-ray diffraction has been investigated experimentally and theoretically. Possibilities for location of impurity atoms in the bulk and the surface layer of single crystals are discussed. The experiments were carried out on silicon crystals of different thicknesses doped with germanium. The general approach for calculation of the fluorescence-yield angular curves has been developed. In the case of the uniform distribution of impurity atoms in the bulk of a crystal and also in the case of the kinematical X-ray diffraction on a thin surface layer, analytical expressions can be used.

1. Introduction

According to dynamical theory, during X-ray diffraction in a nearly perfect crystal X-ray standing waves (XSW) are generated. The period of this wave is equal to or smaller by an integer than the interplanar

0108-7673/90/080649-08$03.00 © 1990 International Union of Crystallography

spacing between reflecting planes (Batterman & Cole, 1964; Kovalchuk & Kohn, 1986). The yield of secondary radiation accompanying X-ray absorption depends on the position of excited atoms with respect to nodes and antinodes of the standing wave. The angular dependence of the host atoms fluorescence yield allows one to determine the Debye–Waller factor for the crystal lattice. Deformation of the surface layer leads to shifts of the surface atoms from their exact positions. For determination of these strains angular dependences of the external photoeffect are used because of a very small yield depth of photoelectrons (Afanas'ev & Kohn, 1978).

High spectral sensitivity of the standing-wave method with measurement of fluorescence yield makes it a very convenient tool for the location of impurity atoms in a crystal lattice. Up to now the problem of location of the impurity or adsorbed atoms has been solved with the use of the Bragg case, when the formation of standing waves takes place in a relatively thin surface layer (Golovchenko, Batterman & Brown, 1974; Materlik & Zegenhagen, 1984; Cowan, Golovchenko & Robbins, 1980). XSW in the Laue case with the registration of secondary radiation from the exit surface have been studied in several papers concerning lattice-atom fluorescence yield (Anaka, 1967) and external (Polikarpov & Yakimov, 1986) and internal (Zheludeva, Kovalchuk & Kohn, 1985) photoeffects. A Laue-case interferometer was used by Materlik, Frahm & Bedzyk (1984) for the location of chemisorbed atoms.

The purpose of the present work is to study the formation of the fluorescence-yield angular curves in the Laue case and the possibilities of this geometry for location of the impurity atoms. As will be shown below, it is possible to study the position of impurity atoms distributed through the bulk of a crystal. In this case the sensitivity of XSW in the Bragg case decreases because of the extinction effect (Batterman, 1964; Patel & Golovchenko, 1983). Moreover, in the Laue case it is easy to use different reflections (including asymmetrical ones) to study the impurity-atom positions in different crystallographic directions.

The experimental results and their qualitative discussion are given in § 2. The method of computing the impurity-atom fluorescence yield from the exit crystal surface in the Laue case is described in § 3. A comparison of the experimental and theoretical curves and the discussion are presented in § 4. Analytical expressions for uniform bulk distribution of impurity atoms and for kinematical diffraction on a thin crystal are discussed also in § 4.

2. Experiment

The experimental arrangement (Fig. 1) was a conventional double-crystal spectrometer in the $(n, -n)$ setting. The first crystal $C1$ diffracting the 111 reflection with Mo $K\alpha$ was asymmetrically cut to increase the angular collimation of the incident beam. The asymmetry factor was $\beta = 1/18$. The sample $C2$ was set in the position of Laue-case (111) diffraction. Mo $K\alpha$ radiation of a conventional X-ray tube was used.

In the first series of measurements we used Si single crystals of different thicknesses with (100) surface orientation uniformly doped during growth with germanium ($N_{Ge} = 7{\cdot}5 \times 10^{25}$ m^{-3}). The 111 Laue reflection in this case was asymmetrical with asymmetry factor $\beta = 0{\cdot}85$ (the angle between the diffracting planes and the crystal surface was 54·7°). Ge $K\alpha$ fluorescence from the exit surface of the silicon crystals was measured by an energy-dispersive Si(Li) detector. The angle between the exit surface and the direction of fluorescence measurements was 60°. An Na(I) detector was used to record the diffracted beam. Because of the very low intensity of the impurity fluorescence yield ($\sim 0{\cdot}3$ counts s^{-1}) the samples were scanned during measurements through the angular diffraction range with the simultaneous registration of the energy region of the Ge $K\alpha$ characteristic peak for each angular point of a diffraction curve (Kazimirov & Kovalchuk, 1987). We used a torsion goniometer, piezoelectric driver and electronic feedback system [similar to the one proposed by Krolzig, Materlik & Zegenhagen (1983)] for scanning and monitoring the sample angular position.

Experimental curves are shown in Figs. 2 and 3. The angular dependence of Ge $K\alpha$ fluorescence yield from a thick crystal with thickness 2·2 mm (Fig. 2) shows a large maximum slightly shifted to the low-angle side with respect to the maximum of the diffracted intensity. On the contrary, in the case of a thin crystal with thickness 0·49 mm, the fluorescence curve (Fig. 3) shows a 'dip' near the center of the reflection range and a weak maximum at the high-angle side. So the curves are quite different. Physical reasons for such behavior will be discussed below. Here we note a very good agreement between the experimental curves (dots) and the theoretical ones (solid lines).

In the second series of measurements we studied Si crystals with thickness 0·35 mm, (111) surface orientation, with an epitaxic layer of 1·6 μm on the exit surface. During growth the epilayer was doped with boron and simultaneously with germanium

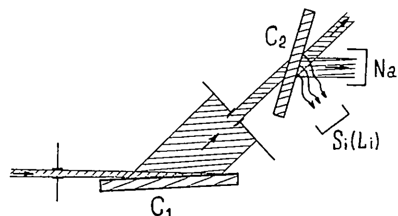

Fig. 1. Experimental arrangement. $C1$ monochromator, $C2$ specimen.

($N_{Ge} = 10^{28}$ m^{-3}). The angle between the surface and the (111) diffraction planes was $\varphi = 70{\cdot}5°$. In this case, the 111 reflection was asymmetrical with asymmetry factor $\beta = \sin(\varphi - \theta_B)/\sin(\varphi + \theta_B) = 0{\cdot}92$ close to unity because of the small value of the Bragg angle $\theta_B = 6{\cdot}5°$.

The experimental curve of Ge $K\alpha$ fluorescence yield from the epilayer in the angular range of diffraction in the substrate is shown in Fig. 4. In this case fluorescence was excited by XSW formed in the bulk of the crystal. An X-ray rocking curve in a wide angular range is shown in Fig. 5(b). One can see that apart from a strong diffraction peak from the substrate there is also an additional weak and broad diffraction peak from the epilayer. This means that as a result of the deformation by impurity atoms (mainly by germanium) the lattice parameter of the epilayer differs from that of the substrate. The deformation in the given crystallographic direction can be estimated as $\Delta d/d = -3{\cdot}8 \times 10^{-3}$. Under X-ray diffraction on the epilayer, the so-called 'kinematical' standing waves are formed in this layer. The fluorescence yield in this angular range is shown in Fig. 5(a). Weak minimum and maximum of the yield were clearly observed on the increasing background. The angular dependence of the background is due to the difference between the plane wave and the wave incident on the layer due to the diffraction in the bulk.

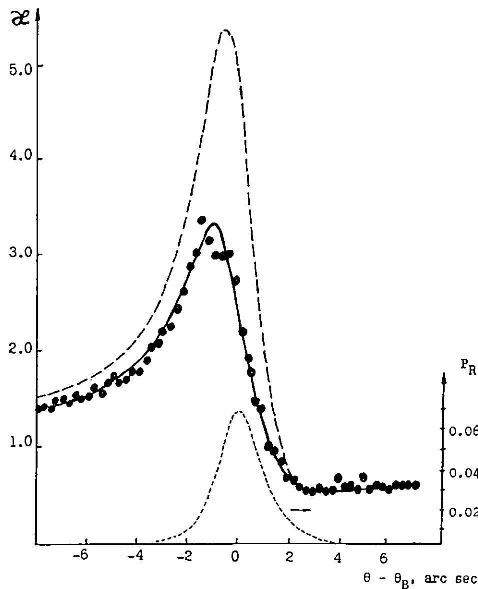

Fig. 2. Angular dependence of the Ge $K\alpha$ fluorescence yield from the Si crystal with $t = 2{\cdot}2$ mm uniformly doped with Ge: circles - experiment; solid line - calculation for substitutional impurity atoms ($u_\nu = 0$); dashed curve - calculation for impurities at $u_\nu = 0{\cdot}15d_{111}$. The X-ray reflection curve P_R is also shown.

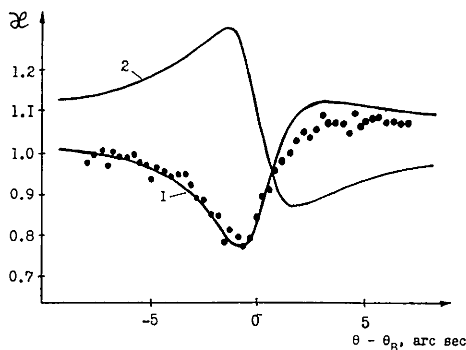

Fig. 3. Angular dependence of the Ge $K\alpha$ fluorescence yield from the Si crystal of $t = 0{\cdot}49$ mm: circles - experiment; curve 1 - calculation for substitutional impurity atoms; curve 2 - calculation for randomly distributed impurities.

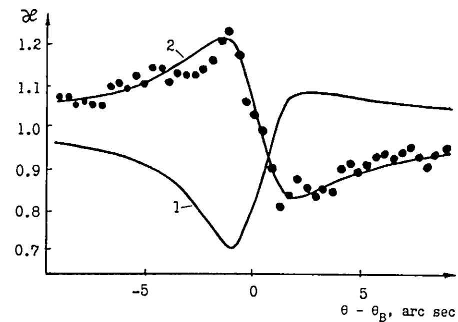

Fig. 4. Angular dependence of the Ge $K\alpha$ fluorescence yield from the epilayer: circles - experiment; curve 1 - calculation for substitutional impurity atoms; curve 2 - calculation for randomly distributed impurities.

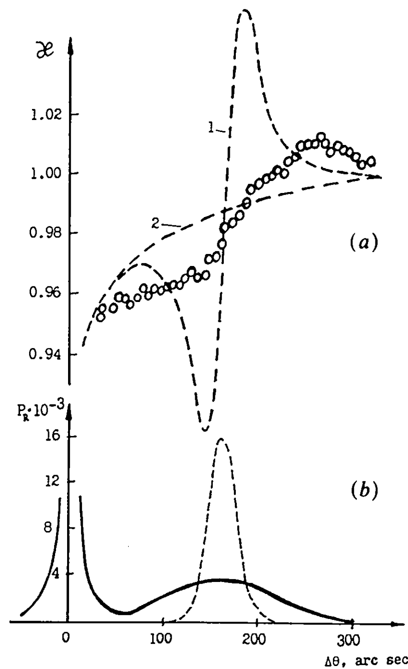

Fig. 5. Angular dependence of the Ge $K\alpha$ fluorescence yield in the angular range of the X-ray diffraction on the epilayer (a) and the corresponding X-ray diffraction curve (b). Dashed lines - calculations for substitutional impurity atoms (1) and for randomly distributed impurities (2).

3. Theory

The theory of secondary-radiation yield excited by X-ray standing waves has been developed in a series of studies in the Bragg case (Batterman & Cole, 1964; Kovalchuk & Kohn, 1986; Afanas'ev & Kohn, 1978) as well as in the Laue case (Anaka, 1967; Zheludeva, Kovalchuk & Kohn, 1985). In a general case the problem is rather complicated and can be solved only by numerical methods. Let us recall the formulation of the task. In the two-beam approximation an X-ray electric-field amplitude has the following form:

$$\mathbf{E}(\mathbf{r}) = \sum_{m=0,h} \sum_{s=\pi,\sigma} E_{ms}(z) \exp(i\mathbf{K}_m\mathbf{r})\mathbf{e}_{ms}, \qquad (1)$$

where $\mathbf{K}_h = \mathbf{K}_0 + \mathbf{h}$, $\mathbf{h}$ is the reciprocal-lattice vector. $E_{0s}(z)$ and $E_{hs}(z)$ for each state of polarization s satisfy the following set of differential equations over coordinate z perpendicular to the crystal surface:

$$\begin{aligned} \mathrm{d}E_0/\mathrm{d}z &= (i\pi/\lambda\gamma_0)[\chi_0 E_0 + C\chi_{\bar{h}} \exp(i\varphi - W)E_h], \\ \mathrm{d}E_h/\mathrm{d}z &= (i\pi/\lambda\gamma_h) \\ &\quad \times[(\chi_0 - \alpha)E_h + C\chi_h \exp(-i\varphi - W)E_0]. \end{aligned} \qquad (2)$$

Here χ_0, χ_h, $\chi_{\bar{h}}$ are the Fourier coefficients of polarizability $\chi = \chi_r + i\chi_i$ of a crystal for X-rays corresponding to the 0, $\mathbf{h}$ and $-\mathbf{h}$ reciprocal-lattice vectors; $C = (\mathbf{e}_{0s}\mathbf{e}_{hs})$ is the polarization factor, $\alpha = -2\sin 2\theta_B(\theta - \theta_B)$, θ is the angle between $\mathbf{K}_0$ and diffraction planes, θ_B is the Bragg angle, $\gamma_0 = K_{0z}/\kappa$, $\gamma_h = K_{hz}/\kappa$, $\kappa = 2\pi/\lambda$, λ is the wavelength of the X-rays. The phase $\varphi(z) = \mathbf{hu}(z)$ is due to the mean displacement of lattice atoms from their positions in an ideal lattice caused by the change of the interplanar spacing, $\exp(-W)$ is the Debye-Waller factor describing static displacements of the atoms from the mean position.

The yield of secondary radiation (Kovalchuk & Kohn, 1986; Afanas'ev & Kohn, 1978) is determined by

$$\begin{aligned} \kappa^{(s,\nu)}(\Delta\theta) = K \int_0^t \mathrm{d}z\, P_\nu(z)(|E_{0s}(z,\Delta\theta)|^2 + |E_{hs}(z,\Delta\theta)|^2 \\ + C_0^{(s,\nu)}(z)\,\mathrm{Re}\,\{E_{0s}^*(z,\Delta\theta)E_{hs}(z,\Delta\theta) \\ \times \exp[i\varphi_\nu(z)]\}), \end{aligned} \qquad (3)$$

where

$$C_0^{(s,\nu)}(z) = 2C\exp[-W_\nu(z)]|\chi_{i\bar{h}}^{(\nu)}|/\chi_{i0}^{(\nu)}. \qquad (4)$$

Here $\Delta\theta = \theta - \theta_B$, t is the crystal thickness, $\chi_{i0}^{(\nu)}$ and $\chi_{i\bar{h}}^{(\nu)}$ are the contributions of atoms emitting the fluorescent radiation to the Fourier coefficients of the imaginary part χ_i of the crystal polarizability. The type of secondary radiation and the type of atoms emitting it are characterized by index ν. Correspondingly, the phase $\varphi_\nu(z) = \mathbf{hu}_\nu(z) + \varphi_{\bar{h}}^{(\nu)}$ and the factor $\exp[-W_\nu(z)]$ relates only to atoms of type ν, $\varphi_{\bar{h}}^{(\nu)}$ is the phase of the complex value $\chi_{\bar{h}}^{(\nu)}$. The function $P_\nu(z)$ describes the yield of secondary radiation of type ν emitted by atoms located at depth z. K is the normalization coefficient chosen so that $\kappa(\Delta\theta) = 1$ at $|\Delta\theta| \to \infty$.

Equations (1)-(4) are general and can be used to analyse a wide range of problems. Below we shall discuss in detail the situation when a crystal can be considered as a set of layers with different lattice parameters, perfections and atomic compositions. A crystal lattice of each layer is characterized by a constant within the layer parameters and $\Delta d/d$, $\exp(-W)$ and $\chi_{0,h}$ describe the change of the plane spacing, decrease of the coherent scattering amplitude and the composition, respectively. Different from Kovalchuk, Kohn & Lobanovich (1985), here we shall be interested only in the Laue case ($\gamma_h > 0$) and the fluorescence yield from the exit surface. In this case $P_\nu(z) = C_\nu \exp[\mu_{yi}(z - t)]$ where $\mu_{yi} = 1/L_{yi}$, L_{yi} is the depth of the fluorescence yield, C_ν is the concentration of impurity atoms.

Let us consider a layer of thickness T at the depth $z_0 < z < z_0 + T$. The phase $\varphi(z)$ in (2) depends linearly on z because $\Delta d/d$ is constant within a layer

$$\varphi(z) = \varphi(z_0) + 2Y\Delta z/L, \qquad (5)$$

where $\Delta z = z - z_0$, Y and L are constant, L is an extinction length averaged over the crystal bulk. The solution of (2) should satisfy the given values of E_0 and E_h on the entrance boundary of a layer.

There are several approaches for solving (2)-(5) with constant values of Y and $\exp(-W)$ within the layer. Below we will use the method developed by Kovalchuk, Kohn & Lobanovich (1985) for the Bragg case. We define the reflectivity amplitude by

$$R(z) = \frac{E_h(z)}{E_0(z)} \frac{\exp[i\varphi(z)]}{(\xi\beta)^{1/2}}, \qquad (6)$$

where $\xi = \chi_h/\chi_{\bar{h}}$, $\beta = \gamma_0/\gamma_h$. The function $R(z)$ satisfies the non-linear equation following from (2):

$$iL(\mathrm{d}R/\mathrm{d}z) = 2bR + C_1(1 - R^2), \qquad (7)$$

where

$$\begin{aligned} b &= y + iy_0 - Y, \\ y &= -\beta^{1/2}\sin 2\theta_B[\Delta\theta - \chi_{r0}(1-\beta)/(2\beta\sin 2\theta_B)]/X, \\ y_0 &= \chi_{i0}(1-\beta)/(2\beta^{1/2}X), \quad X = \lambda(\gamma_0\gamma_h)^{1/2}/\pi L, \\ C_1 &= C(1 - ip)e^{-W}L/L_{\mathrm{ex}}, \\ p &= -\mathrm{Im}\,(\chi_h\chi_{\bar{h}})^{1/2}/\mathrm{Re}\,(\chi_h\chi_{\bar{h}})^{1/2}, \\ L_{\mathrm{ex}} &= \lambda(\gamma_0\gamma_h)^{1/2}/[\pi\,\mathrm{Re}\,(\chi_h\chi_{\bar{h}})^{1/2}], \end{aligned} \qquad (8)$$

with a boundary condition $R = R_0$ on the upper boundary of a layer at $z = z_0$.

The solution of (7) is given by

$$R(z, \Delta\theta) = \frac{X_1 - X_2 D\exp(\sigma\Delta z)}{1 - D\exp(\sigma\Delta z)}, \qquad (9)$$

where

$$D = (X_1 - R_0)/(X_2 - R_0). \qquad (10)$$

Inserting (9) and (10) into (7) and equating to zero coefficients at different powers of $\exp(\sigma\Delta z)$ we obtain

$$X_{1,2}=[b\pm(b^2+C_1^2)^{1/2}]/C_1,\quad \sigma=(2i/L)(b^2+C_1^2)^{1/2}. \tag{11}$$

For simplicity below we will use the branch of the square root of (11) with the positive imaginary part.

Taking (6) into account, the equation for $E_0(z)$ has the following solution:

$$E_0(z)=E_0(z_0)\exp\left(\frac{i\pi\chi_0}{\lambda\gamma_0}\Delta z-\frac{iC_1}{L_{\rm ex}}\int\limits_{z_0}^{z}{\rm d}z_1R(z_1)\right). \tag{12}$$

Inserting (9) and (10) into (12) and performing calculations we have

$$|E_0(z)|^2=|E_0(z_0)|^2|A(\Delta z)|^2|A(0)|^{-2}\exp(-\mu_1\Delta z), \tag{13}$$

where

$$A(\Delta z)=1-D\exp(\sigma\Delta z),\quad \mu_1=\mu_0(1+\beta)/(2\gamma_0)+{\rm Re}\,\sigma. \tag{14}$$

Here $\mu_0=2\pi\chi_{i0}/\lambda$ is the normal absorption coefficient and ${\rm Re}\,\sigma<0$, so μ_1 is the absorption coefficient corresponding to the anomalous transmitted field.

The equations obtained allow us to calculate the contribution of a layer considered in the integral (3). Omitting the calculations, we can write down the result in the form

$$\begin{aligned}\Delta\kappa(T,\Delta\theta)=&\,TP_\nu(z_0)|E_0(z_0)|^2|A(0)|^{-2}\\ &\times(\Psi_1[1+|X_1|^2C_2+{\rm Re}\,(X_1C_3)]\\ &+|D|^2\Psi_2[1+|X_2|^2C_2+{\rm Re}\,(X_2C_3)]\\ &-{\rm Re}\,\{D\Psi_3[2(1+X_1^*X_2C_2)\\ &+X_1^*C_3^*+X_2C_3]\}),\end{aligned} \tag{15}$$

where

$$\Psi_k=[\exp(M_kT)-1]/(M_kT),\qquad M_k=\mu_{yi}-\mu_1+\Delta_k,$$
$$\Delta_1=0,\qquad \Delta_2=2\,{\rm Re}\,\sigma,\qquad \Delta_3=i\,{\rm Im}\,\sigma, \tag{16}$$
$$C_2=|\xi|\beta,\qquad C_3=C_0(\xi\beta)^{1/2}\exp[i(\varphi_\nu-\varphi)].$$

It was assumed in the calculations that the phase difference $(\varphi-\varphi_\nu)$ does not depend on z.

For the case of several layers it is easy to calculate the contribution of each layer using recurrent equations (10), (13) and starting from the entrance surface of crystal, where $E_0=1$ and $R=0$. Note that if layers differ from each other by the atomic composition and the crystal does not have a center of symmetry, then the function $\xi^{1/2}R$ will be continuous but not R. X-ray transmission (P_T) and reflection (P_R) coefficients are given by

$$P_T=|E_0(t)|^2,\qquad P_R=P_T|\xi R(t)|. \tag{17}$$

Equations (8)-(17) were used for computer simulation of the experimental results. Convolution with the first crystal reflection curve was also taken into account.

4. Discussion

First of all we will discuss the experimental results for crystals uniformly doped with impurity (Figs. 2 and 3). In this case the whole crystal can be considered as one layer, so in (15) $T=t$, $D=X_1/X_2$. Moreover, in our experiments we have $L_A\gg L_{yi}\gg L_{\rm ex}$, where $L_A=\gamma_0/\mu_0$. Since $L_{yi}\gg L_{\rm ex}$, the third (interference) term in (15) is very small and we can neglect it ($|\Psi_3|\ll|\Psi_1|, |\Psi_2|$). On the other hand, since $L_A\gg L_{yi}$ the normalized fluorescence yield depends neither on $L_{\rm ex}$ nor on L_{yi}. Taking the above consideration into account we have approximately from (15)

$$\kappa(t,\Delta\theta)\simeq\sum_{k=1,2}I_k(\Delta\theta)\exp[\Delta\mu_k(\Delta\theta)t], \tag{18}$$

where

$$\begin{aligned}I_k&=(1+X_k^2\beta+X_kB)(1+X_k^2)^{-2},\\ X_{1,2}&=[y\mp(y^2+C^2)^{1/2}]/C,\\ \Delta\mu_k&=-X_k\frac{[2C\beta^{1/2}|\chi_{i\bar h}|/\chi_{i0}-X_k(1-\beta)]}{[L_A(1+X_k^2)]},\end{aligned} \tag{19}$$
$$B=2C\beta^{1/2}|\chi_{ih}^{(\nu)}|(\chi_{i0}^{(\nu)})^{-1}\exp(-W_\nu)\cos(2\pi u_\nu/d).$$

To derive (18) we put $\xi=1$, $Y=0$ and used the expansion for the complex parameters X_k in powers of a small value ($|\chi_i|/|\chi_r|$). The parameter u_ν defines shifts of impurity atoms from crystal-lattice nodes in the direction of a reciprocal-lattice vector **h**.

The most significant feature of Laue-case X-ray diffraction is that two types of standing waves are formed in a crystal. One of these waves is a weakly absorbed field with the nodes on the atomic planes, corresponding to the well known Borrmann effect. The other is a strongly absorbed field with the antinodes on the atomic planes. So, as follows from (18), the fluorescence-yield angular curve differs sharply for a thick crystal ($t\gg L_A$) and a thin one ($t<L_A$). The experimental curve shown in Fig. 2 corresponds to $t=4{\cdot}3L_A$. In this case the secondary-radiation yield is excited only by the weakly absorbed X-ray standing-wave field [$k=1$ in (18)]. The other feature of the Laue case is that with rocking a crystal through the reflection position, the standing-wave fields do not move with respect to the atomic planes (as in the Bragg case), but only intensities of these fields increase or decrease. The weakly absorbed field has a maximum intensity at $\theta=\theta_B$ due to the anomalous X-ray transmission. So, even for impurity atoms lying strictly in the crystal nodes ($u_\nu=0$) one can observe increase of the fluorescence yield at $\theta\simeq\theta_B$ in comparison with a background yield. At any displacement from the crystal node, the impurity atom occurs in

the region of the increased field intensity and fluorescence yield increases.

The experimental curve obtained (Fig. 2) is in good agreement with the theoretical one for the model of substitutional impurity-atom position. The maximum normalized fluorescence yield is 3·3. For the impurity atom between the reflecting planes ($u_\nu = d/2$) this value would be 13·9. Note that the sensitivity to the position of the impurity atom increases with increasing crystal thickness. Dependences of the normalized fluorescence-yield maximum on the impurity position with respect to (111) and (022) reflecting planes are shown in Fig. 6 for different crystal thicknesses. The sharper dependence for 022 reflection is due to the enhancement of the Borrmann effect in comparison with 111 reflection. On the other hand, with increasing crystal thickness the background fluorescence yield decreases rapidly. Thus, crystals with intermediate thicknesses, but not too thick, are more appropriate for impurity-location studies. It should be noted that a randomly distributed fraction of impurities also leads to an increase of the fluorescence yield. Indeed, the static Debye–Waller factor for impurity atoms $\exp(-W_\nu)$ and the term $\cos(2\pi u_\nu/d)$ describing coherent displacements are included in (18) as the multipliers. When experimental curves cannot be treated unambiguously, the additional information should be obtained using other reflections, which is easily realized in the Laue case.

For a thin crystal, because of the excitation of both standing-wave fields the situation is more complicated. Both weakly ($k=1$) and strongly ($k=2$) absorbed fields can make a significant contribution to the fluorescence-yield curve, but at different angular positions: field 1 at $\theta < \theta_B$ and field 2 at $\theta > \theta_B$. The main factor now is a degree of interaction of impurity atoms with the standing-wave fields but not the anomalous X-ray transmission. If the impurity atom is in the lattice node, it interacts with field 2 more than with field 1. So, the maximum of the yield will be observed at $\theta > \theta_B$ (curve 1 in Fig. 3). The minimum on curve 1 occurs because field 1 does not interact with impurities and field 2 is not excited in this angular region. If impurity atoms are randomly distributed [in (19), $\exp(-W_\nu) = B = 0$], this effect is compensated for entirely by increasing the interaction with field 1 (curve 2 in Fig. 3). In Fig. 7, one can see the fluorescence yield curves calculated for different positions of impurity atoms. It is obvious that with displacement of the impurity from the diffraction plane interaction with the weakly absorbed field increases and with the strongly absorbed field decreases. So the fluorescence yield increases at $\theta < \theta_B$ and decreases at $\theta > \theta_B$. The experimental curves for both thick and thin crystals unambiguously show that germanium is substitutional in silicon. Such behavior corresponds to the isovalent nature of this impurity.

Now we shall discuss the experimental results obtained with the crystal with the epilayer. The layer thickness $T = 1{\cdot}6$ μm is much less than the extinction length $L_{ex} = 12{\cdot}6$ μm and $t > L_A$. Impurity atoms which are only in the layer 'see' both standing-wave fields and their interference in the angular range of the X-ray diffraction in the substrate. The interference term oscillates with increasing z and the period of these oscillations is different at different values of the incident angle: at $\theta = \theta_B$ the period is equal to πL_{ex} and it decreases with increasing $|\theta - \theta_B|$. Since $t \gg L_{ex}$, the fluorescence-yield angular curve for the case of the incident plane wave strongly oscillates with the period less than the angular divergence of the real incident beam. So, in our treatment of the experimental curve the interference term can be averaged again giving a zero contribution, although the reason

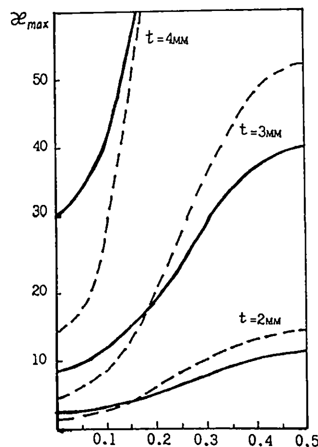

Fig. 6. Theoretical dependences of the maximum fluorescence yield on the position of impurity atoms for silicon crystals of different thicknesses. Solid lines - 111 reflection; dashed lines - 220 reflection.

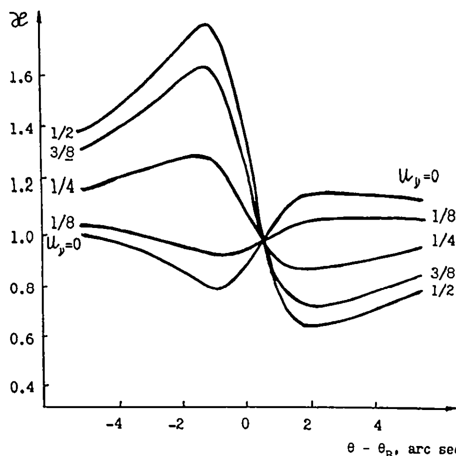

Fig. 7. Calculated angular dependences of impurity fluorescence yield from a thin Si crystal for various impurity positions.

for this averaging is quite different from that of the previous case.

Taking all points above into account, it is clear why the calculated curves in Fig. 4 for substitutional and randomly distributed impurities are very similar to the curves in Fig. 3, although the calculations were carried out in a double-layer model including convolution. But, in this case the experimental curve is in good agreement with the model of random distribution. This means only that impurity atoms are in all possible positions with respect to the standing waves formed in the substrate. Nevertheless, impurities in the layer could be ordered, but with period different from the period of the substrate reflection planes.

It is possible to answer the question of impurity position by measuring the fluorescence-yield curve in the angular range of X-ray diffraction on the epilayer. Since the reflection of X-rays by the epilayer is small ($T \ll L_{ex}$), the standing wave is formed in the layer with intensity weakly oscillating around the average value - the so-called kinematical standing wave. The total reflectivity amplitude in the kinematical approximation is

$$R(z) = Ce^{-W} e^{iqz} \sin(qz)/(iqL_{ex}) + R_0(\Delta\theta + \Delta\theta_B)\, e^{2iqz}, \qquad (20)$$

where coordinate z starts from the upper boundary, $q = -y/L_{ex} = (\pi \sin 2\theta_B/\lambda\gamma_h)\Delta\theta$, $\Delta\theta$ is the angular deviation from the Bragg angle for the layer, R_0 is the reflectivity amplitude of the substrate, $\Delta\theta_B = \theta_B - \theta_B^0$, where θ_B and θ_B^0 are the Bragg angles for the layer and the substrate.

The fluorescence yield from the layer is defined by the general equation (3):

$$\kappa(T, \Delta\theta) = K \int_0^T \mathrm{d}z\, P_\nu(z)|E_0|^2\{1 + |R(z)|^2\beta + C_0\beta^{1/2}\mathrm{Re}\,[R(z)\exp(2\pi i u_\nu/d)]\}, \qquad (21)$$

but at $L_{yi} \gg T$ one can put $P_\nu(z) = 1$ in (21). Moreover, one can consider that the amplitude of the 'incident' wave does not depend on z and this is the 0 component of one of the two standing waves formed in the substrate. Since X-ray diffraction by the layer is observed at $\theta > \theta_B^0$ the 'incident' wave is the 0 component of the strongly absorbed field ($k = 2$). In our case, the shift of the Bragg angle in the layer with respect to the substrate $\Delta\theta_B$ is large enough. It allows us to neglect the h component of the substrate standing wave and put $R_0 = 0$ in the following consideration.

For simplicity we shall discuss two limiting cases: the first one is for randomly distributed impurities ($C_0 = 0$) and the second one is for impurities in crystal nodes ($u_\nu = 0$).

In the first case, substituting (20) into (21) and performing the integration we obtain

$$\kappa(T, \Delta\theta) \simeq K|E_0|^2 T\left[1 + \frac{\beta}{2}\left(\frac{Ce^{-W}}{qL_{ex}}\right)^2 \times \left(1 - \frac{\sin(2qT)}{2qT}\right)\right]. \qquad (22)$$

As follows from (22), on the background yield which increases with increase of $\Delta\theta$ due to the dependence of $|E_0|^2$ on $\Delta\theta$ in the range $\theta > \theta_B^0$, a very weak maximum should be observed with symmetrical shape and intensity proportional to $(T/L_{ex})^2$.

In the second case,

$$\kappa(T, \Delta\theta) \simeq K|E_0|^2 T\left[1 + \frac{\beta^{1/2}C_0 Ce^{-W}}{qL_{ex}} \times \left(1 - \frac{\sin(2qT)}{2qT}\right)\right]. \qquad (23)$$

From (23) quite a different angular dependence of the fluorescence yield follows. It is determined mainly by the interference term and after subtracting the background it has a dispersion form with the maximum at $\Delta\theta > 0$ and the minimum at $\Delta\theta < 0$ both being proportional to (T/L_{ex}). Just such behavior is observed experimentally pointing to the correct positions of germanium in the layer lattice.

The theoretical curves shown in Fig. 5 were calculated using the general approach described in § 3. Both experimental fluorescence-yield curve and X-ray rocking curve are weaker and broader. It is known (Gorbacheva *et al.*, 1986) that a high concentration of germanium in silicon causes the formation of a mosaic structure. This kind of imperfection is the most probable reason for the broadening of the experimental curves.

It was considered previously that X-ray standing-wave fields could be formed only in large and nearly perfect crystals. It is remarkable, as we have demonstrated, that standing waves giving useful structural information can be formed in thin and disordered crystals.

References

AFANAS'EV, A. M. & KOHN, V. G. (1978). *Sov. Phys. JETP*, **47**, 154-161.

ANAKA, S. (1967). *J. Phys. Soc. Jpn*, **23**, 372-377.

BATTERMAN, B. W. (1964). *Phys. Rev. A*, **133**, 759-764.

BATTERMAN, B. W. & COLE, H. (1964). *Rev. Mod. Phys.* **36**, 681-717.

COWEN, P. L., GOLOVCHENKO, J. A. & ROBBINS, M. F. (1980). *Phys. Rev. Lett.* **44**, 1680-1683.

GOLOVCHENKO, J. A., BATTERMAN, B. W. & BROWN, W. L. (1974). *Phys. Rev. B*, **10**, 4239-4243.

GORBACHEVA, N. I., KURBAKOV, A. I., MILVIDSKY, M. G., RUBINOVA, E. E., TRUNOV, V. A. & TUROVSKY, B. M. (1986). *Sov. Phys. Crystallogr.* **31**, 994-996.

KAZIMIROV, A. YU. & KOVALCHUK, M. V. (1987). *Sov. Phys. Crystallogr.* **32**, 428-429.

KOVALCHUK, M. V. & KOHN, V. G. (1986). *Sov. Phys. Usp.* **29**, 426-446.
KOVALCHUK, M. V., KOHN, V. G. & LOBANOVICH, E. F. (1985). *Sov. Phys. Solid State*, **27**, 3379-3387.
KROLZIG, A., MATERLIK, G. & ZEGENHAGEN, J. (1983). *Nucl. Instrum. Methods*, **208**, 613-619.
MATERLIK, G., FRAHM, A. & BEDZYK, M. J. (1984). *Phys. Rev. Lett.* **52**, 441-444.
MATERLIK, G. & ZEGENHAGEN, J. (1984). *Phys. Lett. A*, **104**, 47-50.
PATEL, J. R. & GOLOVCHENKO, J. A. (1983). *Phys. Rev. Lett.* **50**, 1858-1861.
POLIKARPOV, M. A. & YAKIMOV, S. S. (1986). *Sov. Phys. Solid State*, **28**, 907-910.
ZHELUDEVA, S. I., KOVALCHUK, M. V. & KOHN, V. G. (1985). *J. Phys. C*, **18**, 2287-2304.

Acta Cryst. (1990). A**46**, 656-659

The Application of One-Wavelength Anomalous Scattering. I. Combining Results of Different Methods

BY FAN HAI-FU

Institute of Physics, Chinese Academy of Sciences, Beijing 100080, *China*

AND HAO QUAN AND M. M. WOOLFSON

*Department of Physics, University of York, York YO*1 5*DD, England*

(*Received* 2 *December* 1989; *accepted* 7 *March* 1990)

Abstract

Two different techniques for employing one-wavelength anomalous scattering, one using a direct-methods approach and the other a Patterson-like function, are applied to two known protein structures. The first of these, avian pancreatic polypeptide, is in space group $C2$ with one molecule containing 36 amino-acid residues in the asymmetric unit. The second, ribonuclease Sa in space group $P2_12_12_1$, has two molecules each containing 96 amino-acid residues in the asymmetric unit. Both methods give phase indications easily leading to the elucidation of the smaller structure and probably enabling the larger structure to be solved as well. For each structure the electron density maps from the phases given by the two methods are combined through a minimum function. The Fourier transform of the resultant map gives phases better than those given by the individual methods, reducing the mean phase error by 2-3°, which could be critical in some applications.

Introduction

In principle the techniques of multiple isomorphous replacement (MIR) and many-wavelength anomalous dispersion (MAD) enable phases to be determined explicitly and hence structures to be solved. In particular, the MIR method has been very successful for the solution of protein structures; indeed it could be said that the present advanced state of protein crystallography is almost entirely due to this technique. There do occur situations where the MIR technique cannot be applied – for example, when derivatives are not isomorphous with the native product. In such a case the native material may contain a heavy, or fairly heavy, atom such as mercury or zinc and the technique of anomalous scattering is available. Although MAD is then possible (Hendrickson, Pähler, Smith, Satow, Merritt & Phizackerley, 1989), the problem of taking accurate data at different wavelengths with a synchrotron source and then scaling them together does present considerable problems. By contrast one-wavelength anomalous-scattering (OAS) data can be taken much more easily and have been used successfully to solve protein structures.

Techniques for the use of OAS data include combining information from anomalous differences with direct methods (Fan Hai-fu, Han Fu-son, Qian Jin-zi & Yao Jia-xing, 1984) and also use of the P_s function, first introduced by Okaya, Saito & Pepinsky (1955) and further developed by Hao Quan & Woolfson (1989). Examination of the results of applying these two methods reveals that, while they use the same basic data and give mean phase errors of similar magnitude, there are significant differences in the distribution of the errors – so that a reflexion with a large phase error from one technique does not necessarily have a large phase error from the other. This led us to examine the possibility of combining the results of the two techniques to obtain something better than either of them individually; this work is reported here.

0108-7673/90/080656-04$03.00 © 1990 International Union of Crystallography